Negative Energy Consumption of Thermostats at Ambient Temperature: Electricity Generation with Zero Energy Maintenance

J. Wang, J. Shang, and J.P. Huang[*]

Department of Physics, State Key Laboratory of Surface Physics and Key Laboratory of Micro and Nano Photonic Structures (MOE), Fudan University, 200433 Shanghai, China

Thermal maintenance costs 15% of global energy. The concept of an "energy-free thermostat" was accordingly proposed to change environmental temperature gradients, which can maintain a certain space at constant temperature without the need to consume additional energy according to a temperature-trapping theory [Shen *et al.*, Phys. Rev. Lett. 117, 055501 (2016)]. Here we develop the theory by introducing thermoelectric effects, and we then propose a "negative-energy thermostat" that generates electricity associated with energy-free maintenance of a constant ambient temperature. The thermostat further helps to design a different thermoelectric cloak: for changing ambient temperature gradients, its central region has an approximately constant temperature and potential while simultaneously generating thermoelectromotive forces. Our finite-element simulations confirm the effects predicted by the theory developed, and we also discuss the possibility of experimental demonstration with natural materials. This work not only has relevance for expanding the temperature-trapping theory by achieving thermoelectric conversion synergistically but also offers a different method to manipulate coupled fields in electrothermics; it also gives hints on how to control other coupled fields in photothermotics, photoelectrics, electromagnetics, thermomagnetics, and thermomechanics.

I. INTRODUCTION

Thermal phenomena are ubiquitous in nature and daily life. In today's energy-consumption domain, a considerable quantity of heat energy is generated and released as waste energy. On the other hand, about 15% of global energy is used for temperature maintenance or thermal insulation [1]. Hence, how to manipulate heat flow at will is an urgent challenge.

In the past ten years, transformation thermotics has flourished and become a useful tool to control the flow of heat with high efficiency [2–28]. In light of temperature-dependent transformation thermotics (for which thermal conductivities are a function of temperature) [26, 27], the concept of an energy-free thermostat was theoretically proposed and experimentally demonstrated in 2016 [29]. This thermostat keeps a specific region at constant temperature (without the need to consume additional energy) even when ambient temperature gradients change greatly. The underlying mechanism can be understood by a temperature-trapping theory established in Ref. [29]. Based on Fourier's law of heat conduction and the continuity equation of heat flow, the temperature-trapping theory crucially depends on two structures with

asymmetric transitions between good and bad heat conductors. Namely, as ambient temperature gradients increase, one structure changes from a good to a bad conductor, and the other structure changes from a bad to a good conductor. Both structures have the same transition temperature, which is equal to the temperature required to be maintained in the desired specific region.

However, when thermal and electric fields are coupled with each other, the situation could become much more complicated. For example, while the thermostat works at ambient temperature without consuming additional energy, can it generate electricity at the same time? If so, for comparison with previous energy-free thermostats, we call such new thermostats "negative-energy thermostats." For this purpose, here we develop the temperature-trapping theory by introducing thermoelectric effects, which can convert thermal energy into electricity (see, e.g., Ref. [30]). We show, by theory and simulation, that this system can produce thermoelectromotive forces while maintaining the function of a thermostat. Owing to mathematical similarity between thermotics and electrostatics, it is easy to extend the temperature-trapping theory from thermotics to electrostatics by replacement of thermal parameters (thermal conductivity and temperature) with electric counterparts (electric conductivity and potential). As a result, similar effects can be obtained;

---

[*]jphuang@fudan.edu.cn

namely, maintaining a constant electric potential in a specific region while external potential gradients change. On the basis of this, we further design an improved thermoelectric cloak for a model application that not only maintains a constant temperature and electric potential inside the cloaking region, but also outputs thermoelectromotive forces simultaneously. To this end, we also propose a feasible experimental demonstration by adopting commercially available materials, including bismuth telluride (Bi_2Te_3).

II. THEORY AND FINITE-ELEMENT SIMULATION: NEGATIVE-ENERGY THERMOSTAT

Let us consider a one-dimensional case for steady-state heat conduction. In this case, a tripartite structure with a centrosymmetric-logistic-function form of the thermal conductivities of parts A and B could be used for temperature trapping [29]; see Fig. 1(a). The symmetry point is set as T_c. The thermal conductivities of parts A
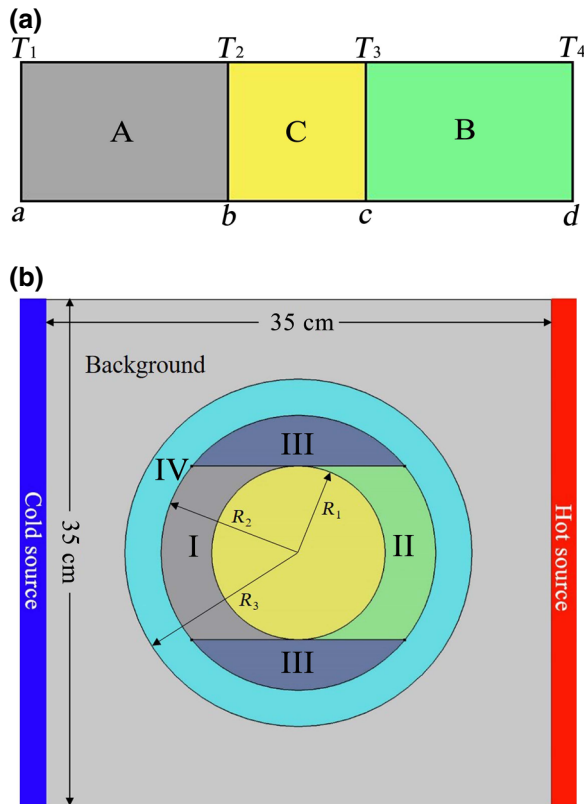

(a)

(b)

FIG. 1. Two schematic graphs. (a) Negative-energy thermostat. Parts A and B possess an additional thermoelectric property with low electric conductivities, while part C has a high electric conductivity. (b) Thermoelectric thermostat cloak located in the center of a background. Regions I and II are occupied by phase-transition materials with the same transition temperature, and regions III and IV are common materials.

and B have a steep but inverse change around this critical temperature. Suppose that parts A and B possess an additional thermoelectric property with a homogeneous isotropic Seebeck coefficient S. The electric conductivities (σ_A, σ_B, and σ_C) of parts A, B, and C are assumed to be three constants satisfying $\sigma_A = \sigma_B \ll \sigma_C$. The correlations of their thermal conductivities follow the same assumption as described in Ref. [29]; relevant details can be found below. Now we are in a position to prove that almost all ambient temperature drops will be occur in parts A and B, thus producing thermoelectromotive forces and forming a constant-temperature zone within part C simultaneously.

Firstly, we build a fundamental model in an open-circuit condition (there is no net current in the circuit). In the one-dimensional system directed along the x axis, the steady-state heat conduction Fourier equation can be expressed as

$$q(x) = -\kappa(T)\frac{dT}{dx} = \text{constant} \rightarrow q(x)dx = -\kappa(T)dT, \tag{1}$$

where q is the density of heat flow along the x direction. As depicted in Fig. 1(a), we have

$$\int_a^b q(x)dx = -\int_{T_1}^{T_2} \kappa_A(T)dT \tag{2}$$

and

$$\int_c^d q(x)dx = -\int_{T_3}^{T_4} \kappa_B(T)dT, \tag{3}$$

where T_1, T_2, T_3, and T_4 (or a, b, c, and d) are corresponding temperatures (or positions along the x axis). Assume that $|b - a| = |d - c|$. Then, on the basis of the law of continuity of heat flow [$q(x)$ is constant at any x position], Eqs. (2) and (3) yield

$$\int_a^b q(x)dx = \int_c^d q(x)dx \rightarrow \int_{T_1}^{T_2} \kappa_A(T)dT$$
$$= \int_{T_3}^{T_4} \kappa_B(T)dT. \tag{4}$$

The thermal conductivities of parts A and B can be assumed to be a centrosymmetric logistic function [29]

$$\kappa_A(T) = \phi + \psi \frac{e^{T-T_c}}{1 + e^{T-T_c}}, \tag{5}$$

$$\kappa_B(T) = \phi + \psi \frac{1}{1 + e^{T-T_c}}, \tag{6}$$

where ϕ and ψ have the same unit as the thermal conductivity (W/m K) and T_c is an arbitrary value between T_1 and

T_4. In Eqs. (5) and (6), a prefactor of $T - T_c$, whose unit is K^{-1}, is omitted throughout this work. For the integral for part A, we obtain

$$\int_{T_1}^{T_2} \kappa_A(T)dT = \phi(T_2 - T_1) + \psi \left(\ln \frac{1 + e^{T_2 - T_c}}{1 + e^{T_1 - T_c}} \right). \quad (7)$$

Considering that T_1 is always much smaller than T_c when heat is conducted from right to left, Eq. (7) can be approximated as

$$\int_{T_1}^{T_2} \kappa_A(T)dT \approx \phi(T_2 - T_1) + \psi \ln(1 + e^{T_2 - T_c}). \quad (8)$$

On the other hand, for the integral for part B, since T_4 is much larger than T_c, we obtain

$$\int_{T_3}^{T_4} \kappa_B(T)dT \approx (\phi + \psi)(T_4 - T_3)$$
$$- \psi[T_4 - T_c - \ln(1 + e^{T_3 - T_c})]. \quad (9)$$

The substitution of Eqs. (8) and (9) into Eq. (4) yields

$$(\phi + \psi)(T_4 - T_3) - \psi(T_4 - T_c) - \phi(T_2 - T_1)$$
$$\approx \psi \ln \left(\frac{1 + e^{T_2 - T_c}}{1 + e^{T_3 - T_c}} \right). \quad (10)$$

Owing to the relationship $\kappa_C \gg \psi \gg \phi$ [29], we have $T_2 \approx T_3$. By ignoring the terms with ϕ (a small quantity), we eventually obtain

$$T_2 \approx T_3 \approx T_c. \quad (11)$$

We have proved that part C is an approximately-constant-temperature zone, and almost all ambient temperature drops will occur in parts A and B. Then the excited thermoelectromotive force ΔU_{ad} can be written as [31]

$$\Delta U_{ad} = \Delta U_{ab} + \Delta U_{cd}$$
$$= S(T_2 - T_1) + S(T_4 - T_3) \approx S(T_4 - T_1). \quad (12)$$

Combining the equation of continuity of heat flow and the equation governing thermoelectric effects, we have theoretically shown a kind of negative energy consumption of thermostats. In this case, parts A and B can be regarded as two batteries in series and the energy comes from the ambient temperature difference between a and d. To show the validity of the above theoretical analysis, we perform finite-element simulations with COMSOL MULTIPHYSICS. We keep the temperature of the cold source constant (273 K) and vary the temperature of the hot source from 320 to 380 K; parts A and B are set to have the Seebeck coefficient $S = 0.2$ mV/K [32]. Figure 2 shows the temperature

distributions [Figs. 2(a)–2(d)] and corresponding potential distributions [Figs. 2(e)–2(h)]. Figures 2(a)–2(d) show that the central temperatures are almost invariant, and are all close to the transition temperature of parts A and B, T_c. On the other hand, the behavior still exists if the temperature of the cold source varies while the hot source is maintained at a constant temperature. In Fig. 4(a), we compare the theoretical thermovoltage with our simulation results (solid line and red stars). This helps to indicate that the proposed model could make nearly full use of ambient temperature gradients for generation of electricity without losing the feature of a thermostat, thus yielding the so-called negative energy consumption of thermostats. The robustness of the theoretical model is verified by the simulation results. In addition, we discuss a possible experimental demonstration in Sec. IV.

We are now in a situation to apply this fundamental model to a practical application scenario (the device is loaded externally). However, the case will be more complex because a net charge-carrier current occurs in the closed circuit. Thus, thermoelectric coupled terms in the governing equations should be taken into account. Here we still consider a one-dimensional system of charge-heat transport. The steady-state Fourier heat conduction Eq. (1) will be modified accordingly as [31]

$$q(x) = -\kappa(T) \frac{dT}{dx} + \Pi j(x), \quad (13)$$

$$j(x) = -\sigma \frac{d\mu}{dx} - \sigma S \frac{dT}{dx}, \quad (14)$$

where $j(x)$ is the electric current density caused by Seebeck effects and μ is the electrochemical potential of each position. Π and S are the Peltier and Seebeck coefficients, respectively, which are assumed to be temperature independent for small temperature gradients. They are regarded as scalar quantities in the one-dimensional case; however, if we consider a three-dimensional anisotropic system, they should be second-order tensors. What is more, Π and S are not independent of each other. They follow the relation of locality $\Pi = TS$ (T is the temperature of the local position) [31]. The first terms on the right-hand side of Eqs. (13) and (14) describe the independent propagation of heat flow and electric current under respective gradients. The second terms are the results of Peltier effects and Seebeck effects. They reveal symmetric and coupled effects in the charge-heat transport. The electric current density $j(x)$ will also cause Joule heating in the circuit and redistribute the temperature of the system in the steady state, which can be described as [31]

$$\frac{dq(x)}{dx} = \frac{j(x)^2}{\sigma} + j(x)S \frac{dT}{dx}. \quad (15)$$
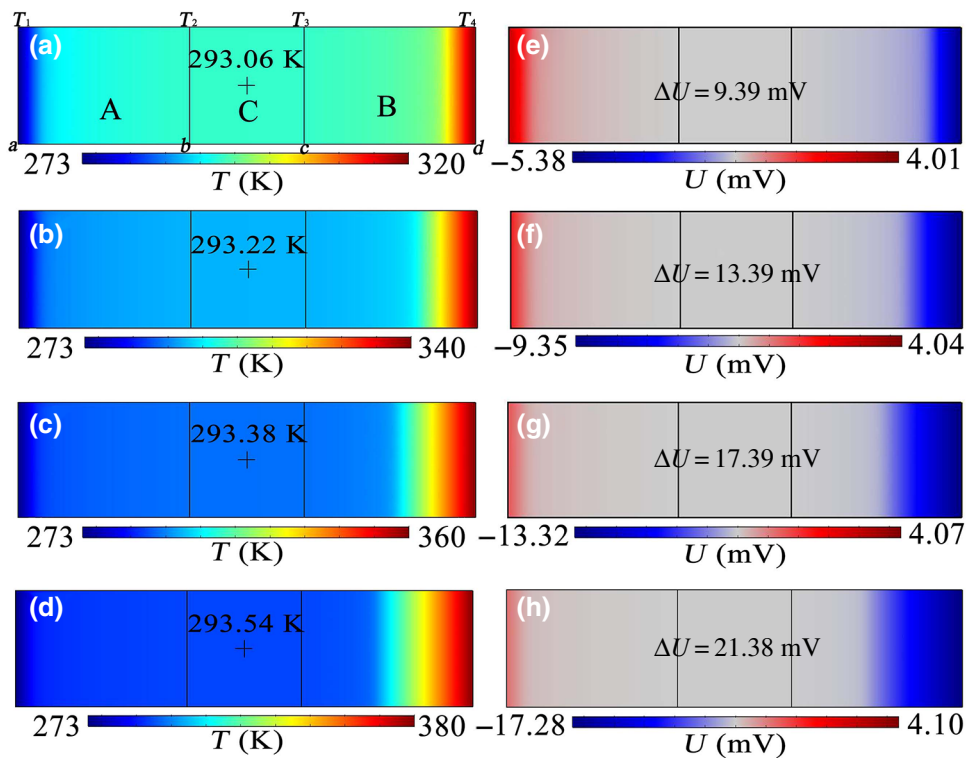
FIG. 2. Temperature (electric potential) distributions based on the model in Fig. 1(a). Parts A and B are 3 cm wide and 2 cm high and part C is 2 cm wide and 2 cm high. We use the Seebeck coefficient $S = 0.2$ mV/K [32] for parts A and B. The electric conductivities of parts A and B are set as $\sigma_A = \sigma_B = 1.1 \times 10^5$ S/m. The thermal conductivities of parts A and B follow Eq. (3) in Ref. [29], where $\delta = 0.4$ W/m K, $\epsilon = 49.6$ W/m K, and $T_c = 293$ K. Part C is occupied by a material with high thermal and electric conductivities ($\kappa_C = 400$ W/m K and $\sigma_C = 1 \times 10^7$ S/m). The upper and lower boundaries are thermally and electrically insulated. The temperatures at the central points [marked with + in (a)–(d)] are indicated within each panel, and the thermoelectric potential differences between the left and right ends in (e)–(h) are extracted and shown within each panel as well.

The coupled thermoelectric governing equations imply an additional hot source due to the Joule-heating effect and a heat flow from the electric current. But the thermoelectric coupled terms will not play an influential role because of the low thermoelectric coefficients Π and S. To prove this, we apply the coupled transport equations to our model and perform finite-element simulations with COM-SOL MULTIPHYSICS. Its thermoelectric module contains Eqs. (13)–(15). When loaded with a conventional resistance (say, its thermal conductivity κ_L and electric conductivity σ_L are low), the thermostat function of the source holds, which is shown in Figs. 3(a)–3(d). The electric load can get part of the thermoelectromotive forces, and its value treads on the heels of the ambient temperature gradients. When we increase κ_L, the central temperature of the source and the voltage drop on the load will be almost unchanged because the source is isolated thermally with two heat or cold reservoirs at both extremes. So the temperature distribution keeps unchanged for the region between the source and the external circuit. However, the variation of σ_L will mainly determine the voltage drop on the

load [Figs. 3(e)–3(h) and 4(a)]. Figures 3(e)–3(h) show the short-circuit case as σ_L and κ_L have the same high values as those of copper interconnects', but the variation of the central temperature of the source is negligible. This can be confirmed by Fig. 4(b). We can see that when the ambient temperature gradient is over 100 K, the difference in central temperatures between the open-circuit case and the short-circuit case is less than 0.02 K. With σ_L increasing, the voltage drop on the load decreases, in accordance with the behavior of the electric power density of the load [Fig. 4(c)]. That is to say, the output electric power of the system has the same trend as the variation of the load's resistance, at least in a very large range. This is because the source's resistance is very high, and the maximum output power is achieved when the resistances of the load and the source are equal [33,34]. We will prove that in our model the energy-conversion efficiency will also be maximum under this condition.

It is the weak coupling effects that make the thermostat source maintain its intrinsic function while outputting electricity. The coupling coefficients are representation signals
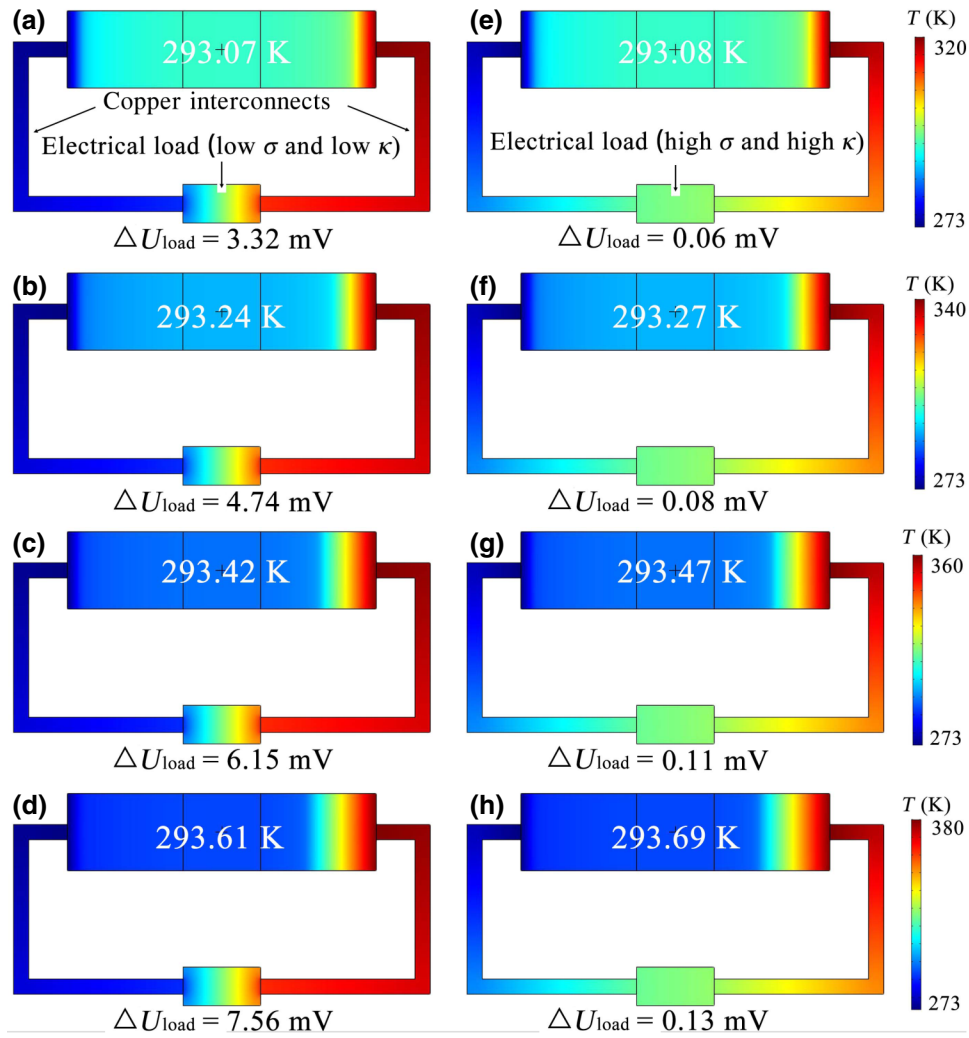
FIG. 3. Temperature distributions while loaded. Copper interconnects and electric load are marked in (a). The temperature of the cold source is kept at 273 K for all simulations and the temperature of the hot source T_h is changed from 320 to 380 K. Each row has the same T_h. The thermal conductivity κ and the electric conductivity σ of the load have the same values in a column but are different between columns. κ of loads in the two columns is 10 and 400 W/m K, respectively, while σ is 1.1×10^5 and 1×10^7 S/m, respectively. κ and σ of copper interconnects are 400 W/m K and 1×10^7 S/m, respectively. The tripartite source has the same thermal and electric parameters as used in Fig. 2. The central temperature of the source and the voltage drop of the load are shown in corresponding locations.

of the strength of coupling. Therefore, the temperature distribution of the whole device will scarcely change. We can define the energy-conversion efficiency of the system as $\eta = W_e/Q_H$, where W_e is the output power and Q_H is the heat flow transferring from the heat reservoir into the source. In our model [Figs. 1(a), 2, and 3], by solving Eqs. (13)–(15) simultaneously, we can obtain

$$Q_H = ST_4 I_e + K_0(T_4 - T_1) - \frac{1}{2}I_e^2 R_0, \quad (16)$$

where K_0 and R_0 are the effective thermal conductance and electric resistance of the tripartite source. As parts A, B,

and C are in series thermally and electrically, by ignoring the influence of part C ($\sigma_C \gg \sigma_A = \sigma_B, \kappa_C \gg \psi \gg \phi$), we can write K_0 and R_0 as

$$K_0 \approx \left[\left(\widetilde{\kappa}_B \frac{A_S}{d-c} \right)^{-1} + \left(\widetilde{\kappa}_A \frac{A_S}{b-a} \right)^{-1} \right]^{-1}, \quad (17)$$

$$R_0 \approx \frac{d-c}{\sigma_B A_S} + \frac{b-a}{\sigma_A A_S}. \quad (18)$$

This is the result of the effective-medium approximation [35]. $\widetilde{\kappa}_B$ and $\widetilde{\kappa}_B$ are the effective thermal
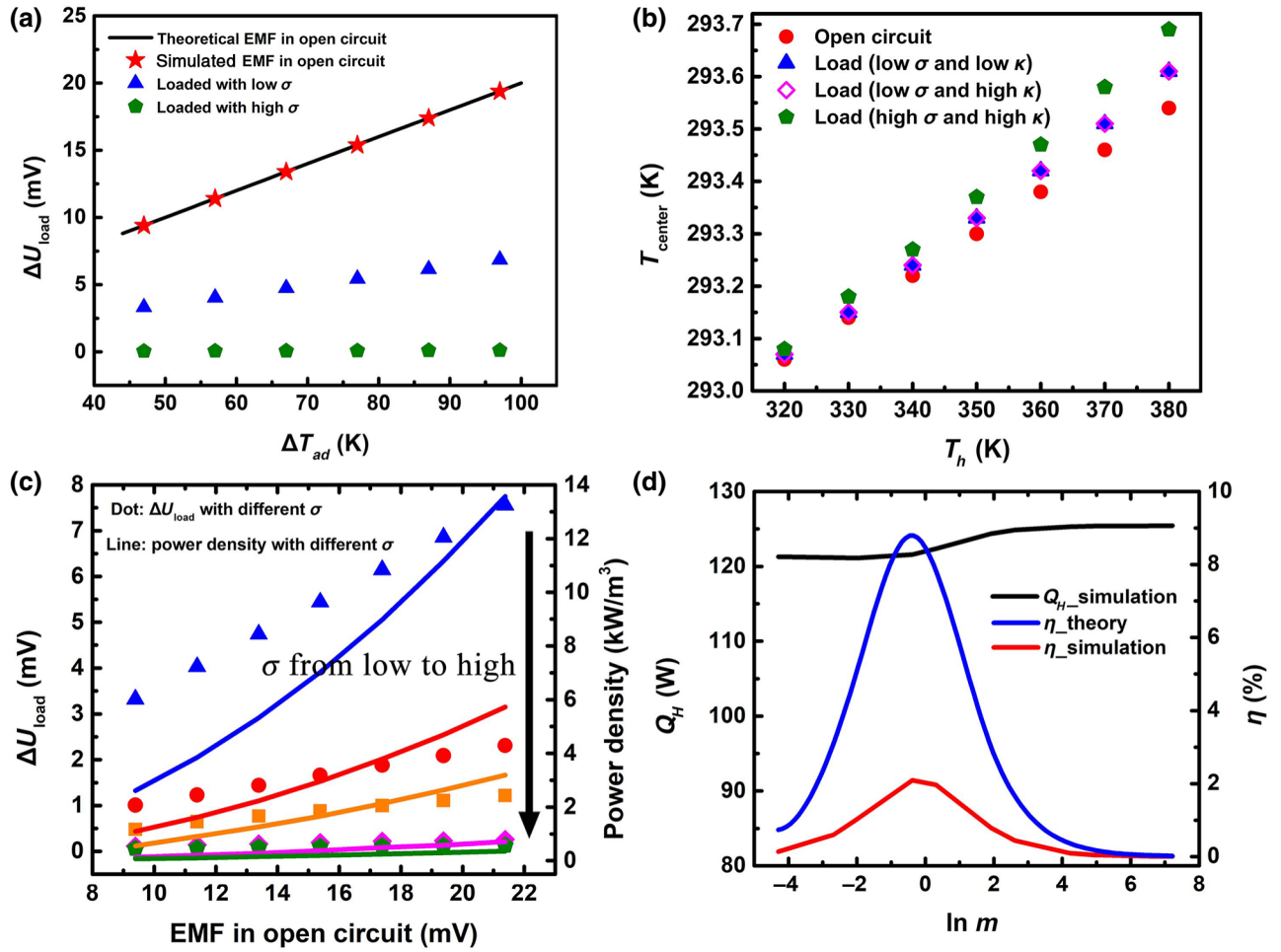
FIG. 4.   (a) Voltage drop of different loads under specified ambient temperature gradients. The electromotive force (EMF) obtained by theoretical calculation [according to Eq. (12) with $\Delta T = T_4 - T_1$; solid line] and simulation (finite-element simulations with COMSOL MULTIPHYSICS; red stars) in the open-circuit case are also shown. (b) The central temperature of different loads versus T_h. (c) The voltage drop and power density of different loads for different working modes of the source. Different σ values are distinguished by different colors. The data in black, red, blue, pink, and green correspond to σ of load of 1×10^7, 5×10^6, 1×10^6, 5×10^5, and 1.1×10^5 S/m, respectively. (d) The energy-conversion efficiency η and the heat flow into the source Q_H versus the logarithm of m. Temperatures of 273 and 380 K are kept at both ends of the source.

conductivities of parts B and A, respectively. They can be deduced as $\widetilde{\kappa_B} = \int_{T_3}^{T_4} \kappa_B(T)dT/(T_4 - T_3)$ and $\widetilde{\kappa_B} = \int_{T_1}^{T_2} \kappa_A(T)dT/(T_2 - T_1)$, respectively. A_S refers to the cross-section area of the source. The first term in Eq. (16) is the heat flow caused by carrier transport, and the second term describes the independent production of the heat flow under temperature gradients. The third term is the result of Joule-heating effects. Its coefficient $\frac{1}{2}$ is based on the assumption that Joule heat flow dissipates to heat or cold reservoirs uniformly. I_e is the electric current in the closed circuit. For convenience of analysis, we set R_L (equal to $l_L/\sigma_L S_L$) as the electric resistance of the load. As the temperature distribution of the source remains almost unchanged under the closed-circuit condition, with use of

Eq. (12) we can obtain

$$I_e = \frac{S(T_4 - T_1)}{R_0 + R_L}. \tag{19}$$

The output power can be given as

$$W_e = I_e^2 R_L. \tag{20}$$

On the basis of Eqs. (16) and (20), we can further write the thermoelectric conversion efficiency of the system as

$$\eta = \frac{W_e}{Q_H} = \frac{I_e^2 R_L}{S T_4 I_e + K_0(T_4 - T_1) - \frac{1}{2} I_e^2 R_0}. \tag{21}$$

Finally, we substitute Eq. (19) into Eq. (21) and get

$$\eta = \frac{T_4 - T_1}{T_4}$$

$$\times \frac{\dfrac{1}{R_0/R_L + 1}}{1 + \dfrac{K_0 R_0(1 + R_L/R_0)}{S^2 T_4} - \dfrac{1}{2}\dfrac{T_4 - T_1}{T_4}\dfrac{1}{1 + R_L/R_0}}. \tag{22}$$

So far, we have deduced the conversion efficiency of our system. When the ambient temperature is fixed, the efficiency is based on the intrinsic property of the source and load. We can define $Z_0 = S^2/K_0 R_0$ as the figure of merit of the source, which describe the source's energy-conversion ability [36]. The effective Seebeck coefficient S of the source approximates that of the bulk Bi_2Te_3 because we can simply infer that $S \approx S_B(T_4 - T_3) + S_A(T_2 - T_1)/T_4 - T_1 \approx S_A = S_B$ according to Eq. (12). So S in the expression for Z_0 of the source is predictable. By setting $m = R_0/R_L$, we can simplify Eq. (22) as

$$\eta = \frac{T_4 - T_1}{T_4}\frac{\dfrac{1}{m + 1}}{1 + \dfrac{1}{Z_0 T_4}\dfrac{m + 1}{m} - \dfrac{1}{2}\dfrac{T_4 - T_1}{T_4}\dfrac{m}{m + 1}}. \tag{23}$$

The simulation results and theoretical efficiency values predicted by Eq. (23) are shown in Fig. 4(d). It gives a qualitative comparison. We keep the temperature of the cold source and the hot source at 273 and 380 K, respectively. The logarithm of m is taken as the horizontal axis. We can see the heat flow Q_H transferring into the thermostat is almost invariable due to the fixed temperature gradients. The trend of the simulation results fits the theoretical calculation of Eq. (23). The difference in values between them is mainly because of the data-extraction approach in COMSOL MULTIPHYSICS (the heat reservoir is coupling with the model and we read the heat-flow density at this position to get Q_H, which is larger than the actual value). In other words, the theoretical calculation is an exact solution, while the simulation result is rough. But together they confirm the conclusion that the efficiency reaches a maximum when $m \approx 1$ or $\ln m \approx 0$. This conclusion is correct only when Z_0 is very small. This can be interpreted by a simple calculation $\partial\eta/\partial m = 0$ and we estimate $m = \sqrt{1 + \frac{1}{2}Z_0(T_1 + T_4)}$ when η is maximum. On the basis of our theoretical calculation of this model, we obtain $Z_0 = 0.0038$ and $Z_0 T = 1.14$ (when $T = 300$ K), which conforms to this condition. We can see Z_0 and m are the determining factors for the conversion efficiency. By redesigning the structure of the negative-energy thermostat (e.g., rearranging the electric connecting in parallel to

reduce the effective electric resistance R_0, so as to increase Z_0 and decrease m) and choosing optimized materials, we can enhance the practical energy-conversion efficiency.

III. THERMOELECTRIC THERMOSTAT CLOAK AS AN EXTENSION TO THE THERMOSTAT

To show the feasibility and applicability of our theory, we apply the theory and further design a homothermal thermoelectric cloak. The cloak can help to transform part of the ambient thermal energy into thermoelectromotive forces, while maintaining approximately constant temperature (or potential) in the central (cloaking) region. In the meantime, it keeps both the temperature distribution and the electric potential distribution outside the cloak from being disturbed.

Cloaking of coupled thermoelectric transport was firstly proposed theoretically in Ref. [37]. Unprecedentedly, a definite method for manipulating coupled thermoelectric domains in a single device was given, which can be generalized to other multiphysics domains. Here we use the core conclusion that the coupling coefficient S remains the same form after coordinate transformation [37]. Combined with the theory of a negative-energy thermostat presented above, we design such a thermoelectric cloak different from the one reported in Ref. [37].

Firstly, as steady heat conduction and electric transport follow the same rule described by Laplace's equation, we can easily generalize the temperature-trapping theory [29] from the thermal domain to the electric domain, thus enabling the trapping of electric potentials in a certain region by the ambient temperature. Secondly, for convenience in manufacturing, we consider a bilayer (two-shell) structure [10]. Thus, as depicted in Fig. 1(b), we use four types of materials for regions I–IV located in a background (with thermal conductivity κ_0 and electric conductivity σ_0). In detail, regions I and II are occupied by temperature-dependent phase-transition materials whose thermal conductivities (κ_I and κ_{II}) and electric conductivities (σ_I and σ_{II}) are described by centrosymmetric logistic functions with a same transition temperature, T_c. That is, the expressions for κ_I, κ_{II}, σ_I, and σ_{II} are as follows:

$$\kappa_I = \phi + \psi\frac{e^{T - T_c}}{1 + e^{T - T_c}},$$

$$\kappa_{II} = \phi + \psi\frac{1}{1 + e^{T - T_c}},$$

$$\sigma_I = \mu + \nu\frac{e^{T - T_c}}{1 + e^{T - T_c}}, \tag{24}$$

$$\sigma_{II} = \mu + \nu\frac{1}{1 + e^{T - T_c}},$$

with $\phi \ll \psi$ and $\mu \ll \nu$. On the other hand, regions III and IV are occupied by two common materials with thermal
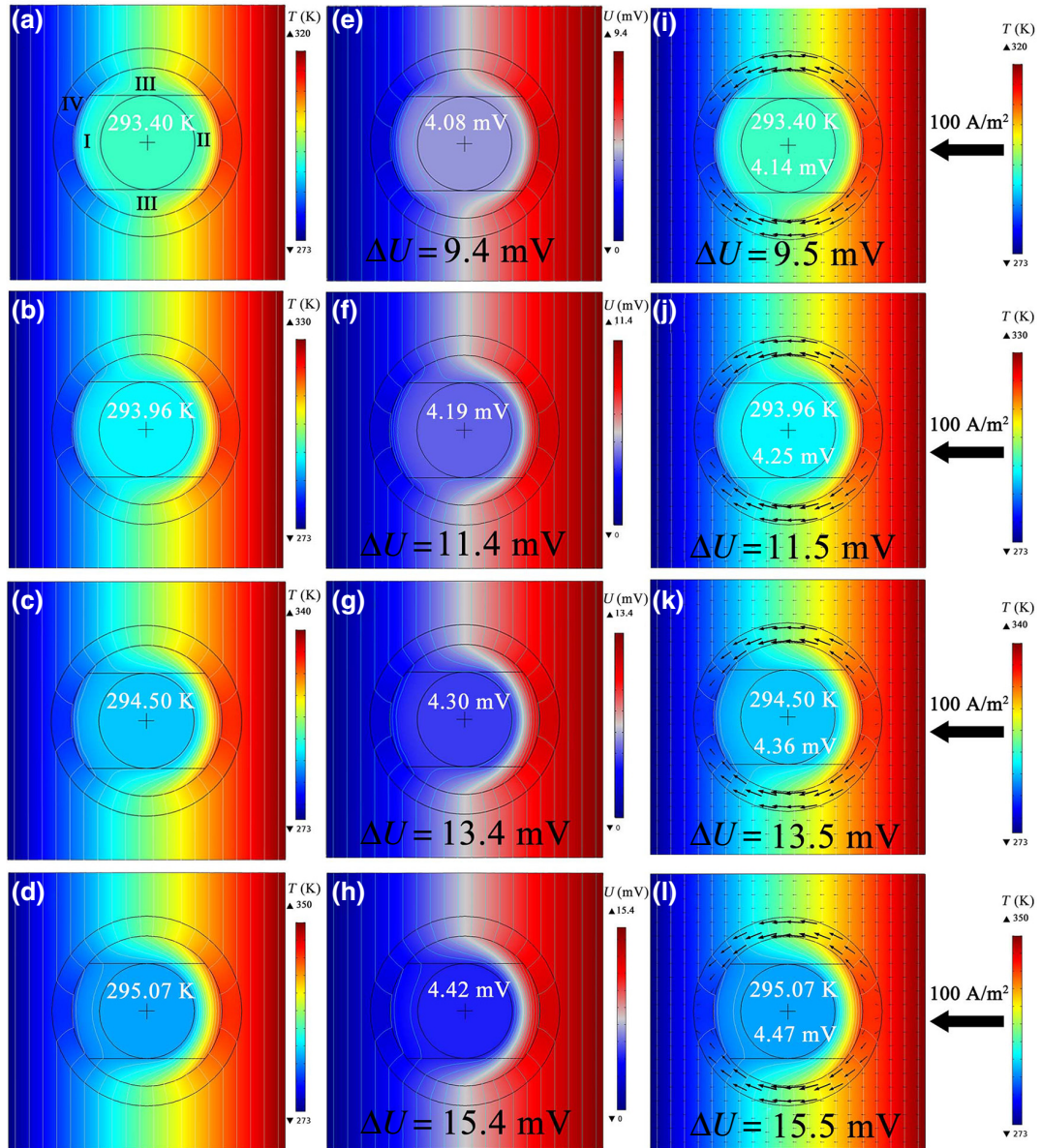
FIG. 5. Results of finite-element simulations of our thermoelectric cloak based on the model shown in Fig. 1(b). Central temperatures or thermoelectric potentials are extracted from the location indicated by + and they are shown in each panel; the potential differences between the right and left ends, ΔU (thermoelectromotive force), are shown in (e)–(l) as well. White lines in (a)–(d),(i)–(l) and blue lines in (e)–(h) indicate isothermal and isopotential lines, respectively. Black arrows in (i)–(l) represent the magnitude and direction of the electric currents. The Seebeck coefficient of the whole region is set as $S = -0.2$ mV/K. Regions I and II satisfy Eq. (24), where $\phi = 0.03$ W/m K, $\psi = 1$ W/m K, $\mu = 3 \times 10^2$ S/m, $\nu = 3 \times 10^4$ S/m, and $T_c = 293$ K. Parameters for regions III and IV follow Eq. (25), where $R_1 = 6$ cm, $R_2 = 9.5$ cm, and $R_3 = 12$ cm. The thermal conductivity of the background $\kappa_0 = 50$ W/m K and the electric conductivity of the background $\sigma_0 = 3 \times 10^5$ S/m.

and electric conductivities given by

$$\kappa_{\text{III}} \to 0,$$

$$\kappa_{\text{IV}} = \kappa_0 \frac{R_3{}^2 + R_2{}^2}{R_3{}^2 - R_2{}^2},$$

$$\sigma_{\text{III}} \to 0,$$

$$\sigma_{\text{IV}} = \sigma_0 \frac{R_3{}^2 + R_2{}^2}{R_3{}^2 - R_2{}^2}, \tag{25}$$

according to the requirement of bilayer cloaks [10]. In addition, we assume that all the regions (namely, regions I–IV together with the central circular region and background) have the same homogeneous isotropic Seebeck coefficient [37].
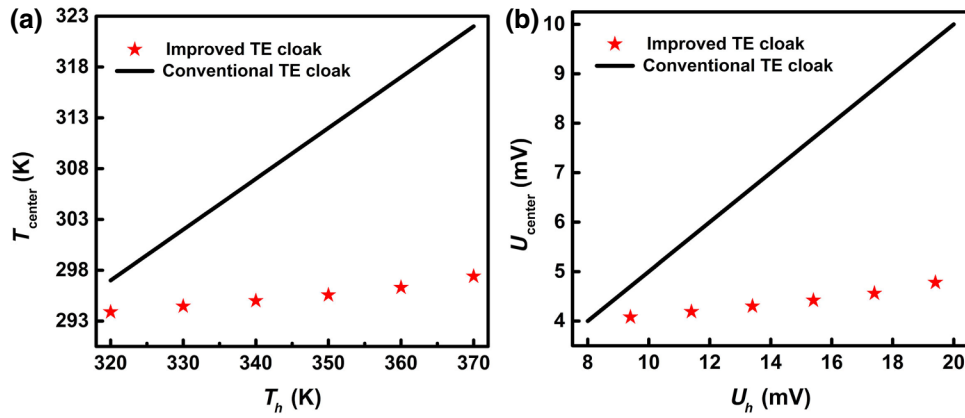
FIG. 6. Comparison of central temperatures and potentials, T_{center} and U_{center}, between our improved thermoelectric (TE) cloak and the conventional thermoelectric cloak [37]. The horizontal axis in (a),(b) represents the temperature (T_h) or potential (U_h) of the right boundary in Fig. 4. Other parameters are described in the text.

The corresponding results of finite-element simulations are shown in Fig. 5. The cold source has a temperature of 273 K and is connected to the ground (with zero potential). The temperature at the central points increases to 1.67 K [Figs. 5(a)–5(d)], while the temperature of the hot source increases from 320 to 350 K. Similar behavior happens for the potential at the central points; see Figs. 5(e)–5(h). However, the thermoelectromotive force increases evidently, as indicated by the big change in ΔU in Figs. 5(e)–5(h), echoing with Eq. (12). What is more, if we keep the above-mentioned condition and input an additional electric current from the right side [see Figs. 5(i)–5(l)], the central temperature and the temperature distribution outside will not be affected. The electric current (black arrows) will steer around the cloaking region and remain uniform as if there were no object existing in the center. The central electric potential will vary slightly because of the additional electric field. The constant electric potential function is not strict because the temperature and the potential are not of equal status in this cloak. Equation (24) implies that the ambient temperature is the key factor to make the thermoelectric cloak a thermostat. So if we apply only a single external electric field at both ends, the cloaking and thermostat function will not work. So this thermoelectric cloak is actually a temperature-driven thermoelectric thermostat cloak.

Thus, under an ambient temperature gradient, one can see that this cloak can not only maintain an approximately constant temperature or potential inside the central region but can also convert heat energy into electricity without disturbing the thermal or electric fields outside as well. Clearly, our thermoelectric cloak is essentially different from the existing thermoelectric cloaks. For the sake of more clarity, Fig. 6 shows the change of temperature or potential at the central points when the temperature of the hot source or the corresponding potential varies significantly. This figure helps to indicate that the central

temperatures and potentials are almost constant, which is in contrast to the linear variation of conventional thermoelectric cloaks designed in Ref. [37].

IV. DISCUSSION AND CONCLUSION

We develop the temperature-trapping theory by taking into account thermoelectric effects. Our application of the theory developed is twofold. Namely, with the help of this theory, we propose the concept of a negative-energy thermostat, and we further design a different kind of thermoelectric cloak with new features.

The so-called negative-energy thermostat means that the thermostat can generate electricity while energy-freely maintaining a constant temperature under ambient temperature differences. On the basis of our theory, we suggest a possible experimental demonstration with details.

A convincing experimental demonstration of energy-free maintenance of temperatures was reported in Ref. [29]: two types of shape-memory alloys were used to realize the symmetric logistic forms of thermal conductivities. For experimental demonstration of the present negative-energy thermostat, we suggest the use of phosphor copper and Bi_2Te_3 (with $\kappa_{Bi_2Te_3} = 1.6$ W/m K and $S_{Bi_2Te_3} = 2 \times 10^{-4}$ V/K, a widely used thermoelectric material [38]). A detailed structure is shown in Fig. 7. Part A or part B has two layers. The bottom layer is composed of three phosphor copper films ($\kappa_p = 54$ W/m K) [39] and three Bi_2Te_3 films. Regarding the top layer, three bimetallic strips composed of phosphor copper films and shape-memory-alloy films are installed above the Bi_2Te_3 locations. They have inverse deformation at the same transition temperatures for parts A and B. Each film or the strip has the same length or width. The Bi_2Te_3 films are slightly thinner than the phosphor copper films for the convenience of leveling the bimetallic strips on the top. The central region contains a copper film ($\kappa_{Cu} = 394$ W/m K).
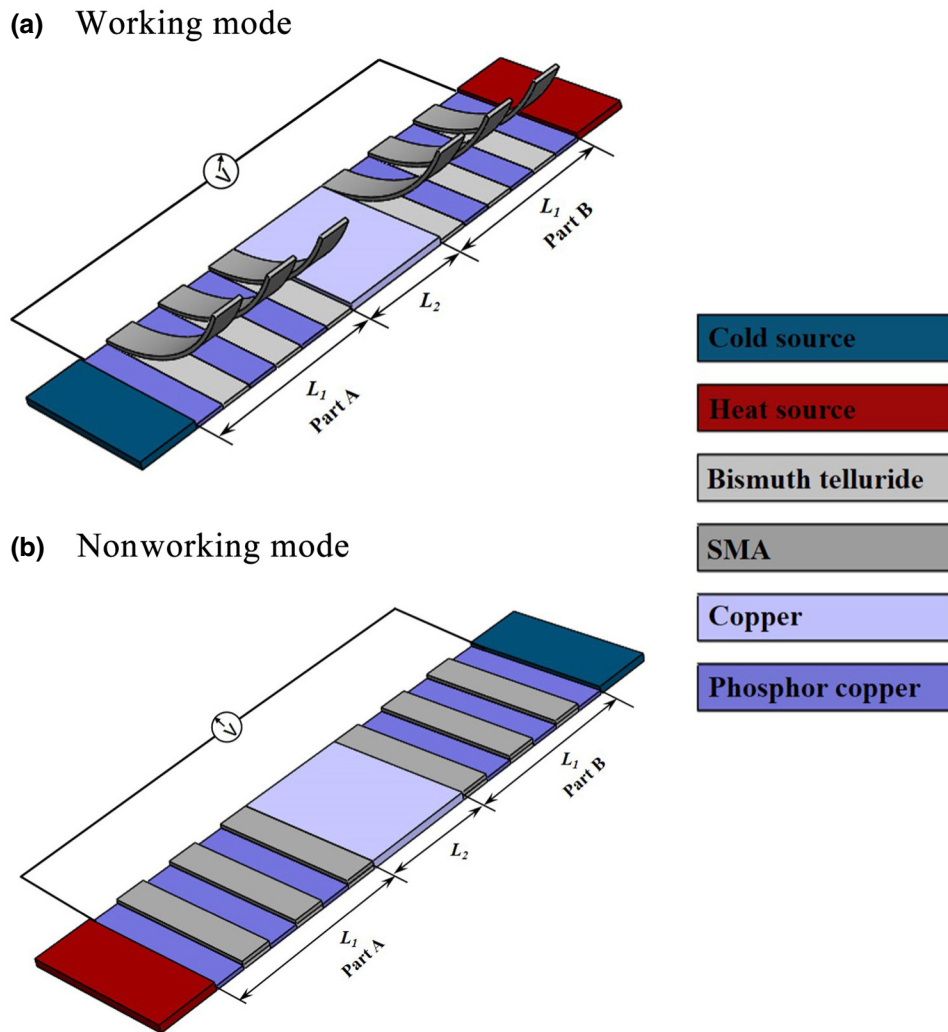
(a) Working mode

(b) Nonworking mode

FIG. 7.   Schematic drawing for possible experimental demonstration on the basis of the experiment reported in Ref. [29]: (a) working mode; (b) nonworking mode. Here we replace silicon grease ($\kappa_s = 4$ W/m K) with Bi_2Te_3 ($\kappa_{Bi_2Te_3} = 1.6$ W/m K and $S_{Bi_2Te_3} = 2 \times 10^{-4}$ V/K). For this design, the thermal-transfer process should be the same as that in Ref. [29], but the new function of generating electricity could be achieved in the working mode.

When the cold (hot) source is placed at the left (right) end, the bimetallic strips will tilt up (level) as a switch of the thermal path. About 97% of the temperature difference will focus on Bi_2Te_3 films (working mode) due to the large thermal-conductivity difference between them and phosphor copper films. So parts A and B play a crucial role in performing the function of converting energy and maintaining temperatures. If the temperature field reverses, this function will disappear and heat flow will run through the bimetallic strips instead of the Bi_2Te_3 films. Then almost no energy will be converted and the temperature of the central region will change with the ambient temperature (nonworking mode). We can calculate the effective thermal conductivities by using the effective-medium theory (see, e.g., Ref. [35]). Accordingly, under the condition of the working mode, the effective thermal conductivity is

3.1 W/m K, while it is 54 W/m K in the nonworking mode. This echoes with Eq. (3) in Ref. [29]. Additionally, the function of production of a thermoelectromotive force can be verified by our probing the electric potential difference between the two ends of the tripartite structure, as demonstrated with voltmeters in Fig. 7.

Inspired by the concept of negative energy consumption of thermostats, we further theoretically design thermoelectric cloaks that differ from those reported in Ref. [37]. When ambient temperature gradients change, our cloaks can not only maintain (approximately) constant temperatures and potentials inside the central region without disturbing thermal or electric fields outside the cloak but can also convert heat energy into thermoelectromotive forces. This idea could be a potential scheme in the design of energy-saving buildings, vehicles, and spacecraft. It can

help create a specific inner environment while collecting and converting energy from the outside. Two problems need to be studied further to achieve the goal of commercial applications. One is to find such practicable multiphysics-environment-responding materials (e.g., thermal and electric conductivities vary synergistically with the temperature). The other is to increase the energy-conversion efficiency. It is worth noting that we focus on steady states in this work. Our thermoelectric cloak works well under this condition. However, for transient states, the situation could become complicated due to the possibility of slight distortion of fields outside [40]. Even so, constant temperatures and potentials can still be maintained inside the cloaking region.

In summary, by developing a different theory to investigate coupled fields in electrothermics, the present work can be considered as a potential green-energy solution. The possibility of expanding this theory to other coupled fields should be verified. This work provides some hints on how to manipulate many other coupled fields, especially those possessing symmetric forms of governing equations as in electromagnetics, thermomagnetics, etc.

[1] E. A. Goldstein, A. P. Raman, and S. H. Fan, Sub-ambient non-evaporative fluid cooling with the sky, Nat. Energy **2,** 17143 (2017).

[2] C. Z. Fan, Y. Gao, and J. P. Huang, Shaped graded materials with an apparent negative thermal conductivity, Appl. Phys. Lett. **92,** 251907 (2008).

[3] T. Y. Chen, C. N. Weng, and J. S. Chen, Cloak for curvilinearly anisotropic media in conduction, Appl. Phys. Lett. **93,** 114103 (2008).

[4] J. Y. Li, Y. Gao, and J. P. Huang, A bifunctional cloak using transformation media, J. Appl. Phys. **108,** 074504 (2010).

[5] S. Guenneau, C. Amra, and D. Veynante, Transformation thermodynamics: Cloaking and concentrating heat flux, Opt. Express **20,** 8207 (2012).

[6] S. Narayana and Y. Sato, Heat Flux Manipulation with Engineered Thermal Materials, Phys. Rev. Lett. **108,** 214303 (2012).

[7] R. Schittny, M. Kadic, S. Guenneau, and M. Wegener, Experiments on Transformation Thermodynamics: Molding the Flow of Heat, Phys. Rev. Lett. **110,** 195901 (2013).

[8] T. C. Han, T. Yuan, B. W. Li, and C.-W. Qiu, Homogeneous thermal cloak with constant conductivity and tunable heat localization, Sci. Rep. **3,** 132 (2013).

[9] H. Y. Xu, X. H. Shi, F. Gao, H. D. Sun, and B. L. Zhang, Ultrathin Three-Dimensional Thermal Cloak, Phys. Rev. Lett. **112,** 054301 (2014).

[10] T. C. Han, X. Bai, D. L. Gao, J. T. L. Thong, B. W. Li, and C.-W. Qiu, Experimental Demonstration of a Bilayer Thermal Cloak, Phys. Rev. Lett. **112,** 054302 (2014).

[11] Y. G. Ma, Y. C. Liu, M. Raza, Y. D. Wang, and S. L. He, Experimental Demonstration of a Multiphysics Cloak: Manipulating Heat Flux and Electric Current Simultaneously, Phys. Rev. Lett. **113,** 205501 (2014).

[12] R. Fleury, F. Monticone, and A. Alu, Invisibility and cloaking: Origins, present, and future perspectives, Phys. Rev. Appl. **4,** 037001 (2015).

[13] K. P. Vemuri and P. R. Bandaru, Geometrical considerations in the control and manipulation of conductive heat flux in multilayered thermal metamaterials, Appl. Phys. Lett. **103,** 133111 (2013).

[14] K. P. Vemuri and P. R. Bandaru, Anomalous refraction of heat flux in thermal metamaterials, Appl. Phys. Lett. **104,** 083901 (2014).

[15] K. P. Vemuri, F. M. Canbazoglu, and P. R. Bandaru, Guiding conductive heat flux through thermal metamaterials, Appl. Phys. Lett. **105,** 193904 (2014).

[16] T. Z. Yang, K. P. Vemuri, and P. R. Bandaru, Experimental evidence for the bending of heat flux in a thermal metamaterial, Appl. Phys. Lett. **105,** 083908 (2014).

[17] X. He and L. Z. Wu, Thermal transparency with the concept of neutral inclusion, Phys. Rev. E **88,** 033201 (2013).

[18] Y. Li, X. Jiang, R. Q. Li, B. Liang, X. Y. Zou, L. L. Yin, and J. C. Chen, Experimental realization of full control of reflected waves with subwavelength acoustic metasurfaces, Phys. Rev. Appl. **2,** 064002 (2014).

[19] L. W. Zeng and R. X. Song, Experimental observation of heat transparency, Appl. Phys. Lett. **104,** 201905 (2014).

[20] Y. Ma, Y. Liu, M. Raza, Y. Wang, and S. He, Experimental Demonstration of a Multiphysics Cloak: Manipulating Heat Flux and Electric Current Simultaneously, Phys. Rev. Lett. **113,** 205501 (2014).

[21] T. C. Han, X. Bai, J. T. L. Thong, B. W. Li, and C.-W. Qiu, Full control and manipulation of heat signatures: Cloaking, camouflage and thermal metamaterials, Adv. Mater. **26,** 1731 (2014).

[22] L. Shen, B. Zheng, Z. Z. Liu, Z. J. Wang, S. S. Lin, S. Dehdashti, E. P. Li, and H. S. Chen, Large-scale far-infrared invisibility cloak hiding object from thermal detection, Adv. Optical Mater. **3,** 1738 (2015).

[23] T. C. Han, X. Bai, D. Liu, D. L. Gao, B. W. Li, J. T. L. Thong, and C.-W. Qiu, Manipulating steady heat conduction by sensu-shaped thermal metamaterials, Sci. Rep. **5,** 10242 (2015).

[24] X. He and L. Wu, Illusion thermodynamics: A camouflage technique changing an object into another one with arbitrary cross section, Appl. Phys. Lett. **105,** 221904 (2014).

[25] J. J. Yi, P. H. Tichit, S. N. Burokur, and André de Lustrac, Converting the patterns of local heat flux via thermal illusion device, J. Appl. Phys. **117,** 084903 (2015).

[26] Y. Li, X. Y. Shen, Z. H. Wu, J. Y. Huang, Y. X. Chen, Y. S. Ni, and J. P. Huang, Temperature-Dependent Transformation Thermotics: From Switchable Thermal Cloaks to Macroscopic Thermal Diodes, Phys. Rev. Lett. **115,** 195503 (2015).

[27] X. Y. Shen, Y. Li, C. R. Jiang, Y. S. Ni, and J. P. Huang, Thermal cloak-concentrator, Appl. Phys. Lett. **109,** 031907 (2016).

[28] R. G. Peng, Z. Q. Xiao, Q. Zhao, F. L. Zhang, Yo. G. Meng, B. Li, J. Zhou, Y. C. Fan, P. Zhang, N.-H. Shen, T. Koschny, and C. M. Soukoulis, Temperature-controlled Chameleonlike Cloak, Phys. Rev. X **7,** 011033 (2017).

[29] X. Y. Shen, Y. Li, C. R. Jiang, and J. P. Huang, Temperature Trapping: Energy-Free Maintenance of Constant Temperatures as Ambient Temperature Gradients Change, Phys. Rev. Lett. **117,** 055501 (2016).

[30] L. E. Bell, Cooling, heating, generating power, and recovering waste heat with thermoelectric systems, Science **321,** 1158899 (2008).

[31] C. A. Domenicali, Irreversible thermodynamics of thermoelectricity, Rev. Mod. Phys. **26,** 1103 (1954).

[32] K. Biswas, J. Q. He, I. D. Blum, C.-I. Wu, T. P. Hogan, D. N. Seidman, V. P. Dravid, and M. G. Kanatzidis, High-performance bulk thermoelectrics with all-scale hierarchical architectures, Nature **489,** 11439 (2012).

[33] G. Benenti, G. Casati, and C. Mejia-Monasterio, Thermoelectric efficiency in momentum-conserving systems, New J. Phys. **16,** 015014 (2014).

[34] G. Casati, L. Wang, and T. Prosen, A one-dimensional hard-point gas and thermoelectric efficiency, J. Stat. Mech. **03,** 03004 (2009).

[35] J. P. Huang and K. W. Yu, Enhanced nonlinear optical responses of materials: Composite effects, Phys. Rep. **431,** 87 (2006).

[36] T. M. Tritt and M. A. Subramanian, Thermoelectric materials, phenomena, and applications: A bird's eye view, Mater, Res. Soc. Bull. **31,** 1557 (2006).

[37] T. Stedman and L. M. Woods, Cloaking of thermoelectric transport, Sci. Rep. **7,** 6988 (2017).

[38] L. Hu, H. Wu, T. Zhu, C. Fu, J. He, P. Ying, and X. Zhao, Tuning multiscale microstructures to enhance thermoelectric performance of n-type bismuth-telluride-based solid solutions, Adv. Energy Mater. **5,** 1500411 (2015).

[39] A. V. Kumanin, A. K. Nikolaev, and N. I. Revina, State diagrams and properties of copper-rich Cu-Fe-P alloys, Rus. Met. **6,** 182 (1987).

[40] S. R. Sophia, X. Bai, B. W. Li, and X. Zhang, Detecting thermal cloaks via transient effects, Sci. Rep. **6,** 32915 (2016).